

## Chapter 9

### SU(1,1) Berry's Phase with Trapped Ions

The time evolution of a quantum system is, of course, completely described by the Schrödinger equation. However, often it is desirable to obtain some sort of intuitive feel for how a given quantum system will evolve under a specified Hamiltonian without having to completely solve the Schrödinger equation. At other times, we may wish to determine how changes in some parameter of the Hamiltonian will effect the time evolution. In such cases, an intuitive understanding of the time evolution is often necessary.

It came as somewhat of a surprise therefore when, in 1984, Berry discovered a rather counter-intuitive phase factor [201, 202] in a rather simple system: one undergoing adiabatic time evolution. This phase factor, and its generalizations, became known as “Berry’s phase.” It was first observed in 1986 [203], in the rotation of polarization of a (classical) light field in a twisted fibre. In this chapter, I will discuss a particular example of a so-called “quantum Berry’s phase” [204, 205, 206, 207] which should be observable in the motion of a trapped ion subject to squeezing operations (see Sec. 6.1.4). I will start out by describing Berry’s original observation and the subsequent generalizations of his work. Then, I will use a more modern approach to describe a Berry’s phase in a simple system: a spin-1/2 particle in a magnetic field. Finally, I will use the language which has been developed in the early part of the chapter to describe the Berry’s phase due to squeezings, and a possible future experimental implementation of the measurement.

## 9.1 Berry's Phase

In order to understand the historical context in which Berry's phase arose, let us consider, as he did, a quantum system in an eigenstate of its Hamiltonian:  $\hat{H}|\phi_n\rangle = E_n|\phi_n\rangle$ . If  $\hat{H}$  is slowly changed<sup>1</sup> then, according to the adiabatic theorem [208], the system remains in the  $n^{\text{th}}$  eigenstate of the slowly-changing Hamiltonian  $\hat{H}(t)$ . If we change the Hamiltonian so that at time  $\tau$  it returns to its initial form,  $\hat{H}(\tau) = \hat{H}(t=0)$ , it follows that the system must return to the state described by  $|\phi_n\rangle$ : that is, the system must return to its initial state. However, state vectors are arbitrary up to a phase factor of modulus unity. So in general, under the course of the system's evolution, we must write  $|\phi_n\rangle \rightarrow e^{i\theta}|\phi_n\rangle$ , where  $\theta$  is some phase. Indeed, we may express the state of the system at time  $\tau$  as:

$$|\psi_n(\tau)\rangle = e^{-\frac{i}{\hbar} \int_0^\tau E_n(t') dt'} e^{i\gamma_n(\tau)} |\phi_n\rangle. \quad (9.1)$$

The first exponential is simply the usual dynamical phase induced in the eigenstate through the time evolution operator: the time integral merely reflects the fact that the  $n^{\text{th}}$  eigenstate's energy may be (and probably is) time dependent as we vary the Hamiltonian. This is the phase factor which we would first think to write down in describing the dynamics of the system. The second phase factor,  $\gamma_n(\tau)$ , accounts for any "unexpected" phases which may crop up in the situation described: as we shall see (and as Berry first pointed out), this term is generally nonzero.

At any point in the system's evolution, we may write an equation similar to Eq. (9.1):

$$|\psi_n(t)\rangle = e^{-\frac{i}{\hbar} \int_0^t E_n(t') dt'} e^{i\gamma_n(t)} |\phi_n(t)\rangle. \quad (9.2)$$

where  $|\phi_n(t)\rangle$  is the  $n^{\text{th}}$  eigenstate of  $\hat{H}(t)$ . From the Schrödinger equation, we have that

$$i\hbar \frac{\partial |\psi_n(t)\rangle}{\partial t} = E_n(t) |\psi_n(t)\rangle. \quad (9.3)$$

---

<sup>1</sup> For example, in a magnetic system, we might slowly change the direction of the magnetic field.

Thus, writing  $\xi_n(t) = -(1/\hbar) \int_0^t E_n(t') dt'$ , differentiating Eq. (9.2), and plugging into the Schrödinger equation, we obtain:

$$i\hbar \left[ -\frac{i}{\hbar} E_n(t) e^{i\xi_n(t)} e^{i\gamma_n(t)} |\psi_n(t)\rangle + i e^{i\xi_n(t)} e^{i\gamma_n(t)} \frac{d\gamma_n(t)}{dt} |\psi_n(t)\rangle + e^{i\xi_n(t)} e^{i\gamma_n(t)} \frac{\partial}{\partial t} |\psi_n(t)\rangle \right] = e^{i\xi_n(t)} e^{i\gamma_n(t)} E_n |\psi_n(t)\rangle, \quad (9.4)$$

or,

$$\frac{\partial}{\partial t} |\psi_n(t)\rangle + i \frac{d\gamma_n(t)}{dt} |\psi_n(t)\rangle = 0. \quad (9.5)$$

Multiplying on the left by  $\langle \psi_n(t) |$ , we finally have:

$$\frac{d\gamma_n(t)}{dt} = i \langle \psi_n(t) | \frac{\partial}{\partial t} |\psi_n(t)\rangle. \quad (9.6)$$

so that, in changing the Hamiltonian adiabatically from its initial configuration and then returning it to that initial configuration (for which  $\gamma_n(0) = 0$ , by definition), we have:

$$\gamma_n(\tau) = i \int_0^\tau \langle \psi_n(t) | \frac{\partial}{\partial t} |\psi_n(t)\rangle dt. \quad (9.7)$$

Now suppose that the time dependence of the Hamiltonian arises because we are changing some parameter or parameters  $\mathcal{R}$  with time. In this case, we may re-express Eq. (9.7) as:

$$\begin{aligned} \gamma_n(\tau) &= i \int_0^\tau \langle \psi_n | \frac{\partial}{\partial t} |\psi_n\rangle dt \\ &= i \int_{\mathcal{R}_0}^{\mathcal{R}_f} \langle \psi_n(\mathcal{R}) | \nabla_{\mathcal{R}} \psi_n(\mathcal{R}) \rangle d\mathcal{R}, \end{aligned} \quad (9.8)$$

which was Berry's result. By applying Stokes' theorem to the integral of the divergence, Berry pointed out that the phase factor  $\gamma_n$  could be interpreted as a surface integral over the closed loop in parameter space traced out by the Hamiltonian in the course of its evolution. From these considerations, it becomes apparent that the phase depends *only on the path taken* in the configuration space of the parameters  $\mathcal{R}$ .<sup>2</sup> So this phase does

---

<sup>2</sup> This implies that if the Hamiltonian depends only on one parameter, then the Berry's phase vanishes, since the integral always vanishes in the one-dimensional case: the curve subtends no area.

not depend, for example, on the amount of time taken to return these parameters to their original values. This is in stark contrast to the dynamical phase, which is explicitly time-dependent. In this sense, the Berry's phase is "surprising" [201].

It is interesting to note that the Aharonov-Bohm effect [209] may be interpreted as a Berry's phase [201]. Also, the properties of a spin in a slowly-varying magnetic field may be interpreted in a similar way [201]. In particular, evaluating Berry's phase for the case in which the spin-1/2 particle adiabatically follows a magnetic field which is rotated in its direction by  $2\pi$  shows that the state vector for the spin-1/2 particle picks up a phase factor of -1 during this effective  $2\pi$ -rotation of the particle: this is an example of the well-known behaviour of fermions under rotations.

As might be expected from the above remarks, Berry's treatment may be generalized, and treated in a purely geometric manner. Some of the first steps in this generalization were made by Aharonov, Anandan, and Stodolsky [210, 211, 212]. They removed the requirement of adiabaticity in the change of the Hamiltonian, and showed that even in this case, the phase factor could be interpreted purely in terms of the inherent geometry underlying the changes in the Hamiltonian. As interest in Berry's phase (now also frequently called the "geometric phase") grew, a clearer picture of the situation arose, and a more concise language for describing the physics was developed. An overview of the geometric phase, and a "grammar" of the language, is given by Jordan [213]. In the next section, I will use this modern formulation to describe a canonical example of a geometric phase: the behaviour of a spin-1/2 particle in a magnetic field. Hopefully, this example will clarify the situation, and set the stage for discussing the geometric phase induced by squeezing operations.

It is worth noting that, after Berry's paper came out and the geometric interpretation of his result became apparent, it was pointed out that similar results existed in classical systems: in particular, the connection was drawn [214] with Panchatnaram's phase in classical polarization optics [215] and with the Hannay angle of classical me-

chanics [216, 217]. In general, such phase angles arise whenever a system’s dynamics are constrained in a non-trivial, “geometric” fashion. Such angles are examples of *anholonomies* [218]. A simple example may help to define the word. Consider a set of Cartesian coordinate axes constrained to move on the surface of a sphere, such that the  $z$ -axis is initially pointing in the direction of the north pole. Now, suppose that we translate the axes along the sphere in a parallel-transport fashion (such that we never explicitly rotate the coordinate axes about the  $z$ -direction). If we eventually bring the coordinate frame back to the north pole then, although we have *never* rotated the frame about the normal axis to the sphere, we will find that the coordinate system has undergone a net rotation about this axis! (One may try this out, using an imaginary sphere and one’s fingers as the coordinate frame — provided one is careful not to injure one’s self!) The reason for this rotation is that the coordinate frame is constrained to move on an inherently curved surface: the surface of a sphere. The rotation of a coordinate frame upon completion of a closed circuit on a curved surface is called “anholonomy.”

Of course, as the example indicates, anholonomy effects exist in classical physics. The difference with quantum systems is that quantum systems may exhibit superposition and interference effects. Such effects are phase-sensitive. So, in a single-particle quantum system, the Berry’s phase may have physical effects.

## 9.2 An Example: a Spin-1/2 Particle in a Magnetic Field

In order to introduce the terminology which I will later use to discuss the geometric phase induced by squeeze operators, let us consider a situation which may be somewhat more familiar to atomic physicists: the case of a spin-1/2 particle in a magnetic field. Of course, the time evolution in such a system may be described by the Schrödinger equation or the Bloch equations: such solutions are well known. However, here I will introduce another point of view which distinguishes the “geometric” phase

from “dynamical” phases. This will highlight the different types of evolution inherent in the dynamics. Furthermore, the language I will use is applicable to other, more complicated quantum systems.

Let the magnetic field  $\mathbf{B}(t)$  initially lie along the  $z$ -direction:  $\mathbf{B}(t = 0) = B\mathbf{e}_z$ . Thus, the initial Hamiltonian is given by

$$\hat{H}(t = 0) = -\mu_B \mathbf{B}(0) \cdot \hat{\mathbf{S}} = -\mu_B B \hat{S}_3, \quad (9.9)$$

where (as in Ch. 3),  $\hat{S}_3 = \frac{1}{2}\hbar\hat{\sigma}_3$  is the spin angular momentum operator in for the  $3 \equiv z$  direction.<sup>3</sup> Assume that the particle initially starts out in an eigenstate of  $\hat{S}_z$ . The question is then to determine what happens to the particle if the direction of the  $B$ -field is then rotated in some matter such that, at time  $t = \tau$ , the field again lines up with the  $z$ -axis.

It is somewhat easier conceptually to consider the problem in the Heisenberg picture. In particular, as we shall see, this picture admits a geometric interpretation not only of the phase, but also of the various physical observables of the system and their inter-relationship with the geometric phase. In the Heisenberg picture, the state vector remains constant while the operators evolve in time, according to:

$$\dot{\hat{O}} = -\frac{i}{\hbar}[\hat{H}, \hat{O}], \quad (9.10)$$

which is the Heisenberg equation of motion. So in order to track the changes in physical observables of an initial eigenstate of  $\hat{S}_3$  as the magnetic field is rotated, it suffices to see what happens to the operator  $\hat{S}_3$ .

The idea, then, is that we start out with the operator  $\hat{S}(t = 0) = \hat{S}(0) = \hat{S}_3 \propto \hat{H}(t = 0)$ , and apply unitary transformations  $\hat{U}(t)$  to this operator. The unitary trans-

---

<sup>3</sup> Note that I am continuing to use the notation  $\hat{S}_1, \hat{S}_2, \hat{S}_3$  as I did in Ch. 3. This is an attempt to avoid confusion with the standard use in the rest of this thesis of  $x, y,$  and  $z$  as principal directions in the trap. Of course, here there *is* a physical correspondence between the Pauli operators and physical directions:  $1 \leftrightarrow x, 2 \leftrightarrow y,$  and  $3 \leftrightarrow z$ .

formations are generated by operators which I will label  $\hat{G}(t)$ , so that:

$$i\frac{d}{dt}\hat{U}(t) = \hat{G}(t)\hat{U}(t). \quad (9.11)$$

The change in the original operator  $\hat{S}(0) = \hat{S}_3$  is then given by:

$$\hat{S}(0) \longrightarrow \hat{S}(t) = \hat{U}(t)\hat{S}(0)\hat{U}^\dagger(t). \quad (9.12)$$

In our case, we will consider rotations of the magnetic field  $\mathbf{B}$  away from the  $z$ -direction. These rotations are described by unitary operators  $\hat{U}(t)$ , and the generators of the unitary operators are just the angular momentum operators  $\hat{S}_1$ ,  $\hat{S}_2$ , and  $\hat{S}_3$ <sup>4</sup>, satisfying the usual commutation relations:

$$[\hat{S}_i, \hat{S}_j] = i\varepsilon_{ijk}\hat{S}_k. \quad (9.13)$$

So, in our situation, the operators  $\hat{G}(t)$  are the spin-1/2 angular momentum operators (and combinations of them). The unitary rotation operator,  $\hat{U}(t)$ , then generically will be of the form:

$$\hat{U}(t) = e^{i\mathbf{n}(t)\cdot\mathbf{S}} = e^{n_1(t)S_1+n_2(t)S_2+n_3(t)S_3}, \quad (9.14)$$

which is just the general expression for a rotation operator operating in the angular momentum 1/2 manifold [219].

Now, the rotation operators form a group: the rotation group. The defining property of this group is that it preserves the dot product, and hence the norm. So, for example, if rotation operators act upon a vector  $\mathbf{v} = v_1\mathbf{e}_1 + v_2\mathbf{e}_2 + v_3\mathbf{e}_3$ , then the length of the vector does not change:  $|\mathbf{v}|^2 = (v_1)^2 + (v_2)^2 + (v_3)^2 = \text{const}$ . The generators (the  $\hat{S}_i$ ) of the rotation group form a Lie algebra: in our case, the Lie algebra SU(2) of the Pauli matrices. But there is a very intimate relationship between Lie algebras and (non-Euclidean) geometry. This should not be too surprising: the Lie algebra gives the mathematical properties of infinitesimal changes under the action of some group

---

<sup>4</sup> which also happens to be our  $\hat{A}(0)$

when acting upon vectors, and so should give the “allowable” changes in the vectors with that group — in other words, a geometry. In any event, this implicit geometry will give us a picture of the various changes in phase under the action of the changing spin Hamiltonian. In this case, the picture is just another way of obtaining the Bloch sphere.

The rotation group causes rotations of vectors in any vector space, of any dimension, upon which it operates (for example, in quantum mechanics, one has the various manifolds for different values of the angular momentum). But there is one special vector space associated with the rotation group. This “special” vector space is that spanned by the three generators of the rotation group: the generators form an algebra, and an algebra is a particular example of a vector space [220]. So, although there are many different representations of the rotation group [221], the one obtained by considering a vector space whose dimension is equal to the number of group generators is special: this representation gives us the geometry associated with that group. I will now sketch out how this occurs.

Consider the operators  $\hat{S}_i$  as vectors in a three-dimensional vector space. These three vectors form a basis for that vector space: that is, any general vector may be expressed as:

$$\hat{S} = s_1\hat{S}_1 + s_2\hat{S}_2 + s_3\hat{S}_3. \quad (9.15)$$

We may construct a geometry in this vector space by examining the commutation relations, Eq. (9.13). In the language of Lie algebras, the  $\varepsilon_{ijk}$  are known as the *structure constants* of the Lie algebra [222], and these structure constants carry with them geometrical information. For example, let  $\hat{S}_a = \sum(s_a)_j\hat{S}_j$  and  $\hat{S}_b = \sum(s_b)_j\hat{S}_j$  be two vectors in our vector space. Then it is easy to verify that

$$[\hat{S}_a, \hat{S}_b] = s_1\hat{S}_1 + s_2\hat{S}_2 + s_3\hat{S}_3, \quad (9.16)$$

where

$$s_k = (s_a)_i (s_b)_j \varepsilon_{ijk} \quad (9.17)$$

(using the Einstein summation convention). This expression is identical to the usual component expansion of the vector cross product! So there is an equivalence between the commutator and a vector cross product in the vector space:

$$[\hat{S}_a, \hat{S}_b] \longleftrightarrow \hat{S}_a \times \hat{S}_b, \quad (9.18)$$

The “cross product” is induced by the structure constants of the Lie algebra (in this case, the usual Levi-Civita symbol,  $\varepsilon_{ijk}$ ).

Thus, the structure constants, the Levi-Civita symbol, induce a vector product (or, more generally, an “exterior product”) upon the vector space. The geometric implications of the Levi-Civita symbol goes further. A Lie algebra result [222] shows that this set of structure constants also induces a dot product (or “inner product”) upon the vector space, according to:

$$\hat{S}_a \cdot \hat{S}_b = (S_a)_i (S_b)_j \delta_{ij} \quad (9.19)$$

$$\delta_{ij} = -\frac{1}{2} \varepsilon_{ikl} \varepsilon_{jlk}. \quad (9.20)$$

For the rotation group,  $\delta_{ij}$  is just the usual Kronecker delta which is associated with the usual dot product.

From this, we see that the geometry induced by the group of rigid rotations upon the vector space of the Lie algebra of the group generators is just the usual Euclidean geometry which we associate with real, three-dimensional space. This is not terribly surprising: rotations are one part of the “Galilean” group of symmetries of regular, three-dimensional Euclidean space. In general, however, if we try to apply a similar “geometry-finding” procedure to other groups and their generators, the geometry which we’ll find will *not* be Euclidean. In particular, as we shall see, the group of squeezings will be generated by the Lie algebra  $SU(1,1)$ , and the geometry will be that of Minkowski spaces.

Meanwhile, let us return to our spin-1/2 particle in a magnetic field. We start out in an eigenstate of  $\hat{S}_3$ , and apply a series of rotations. In the Heisenberg picture, we start out with the operator

$$\hat{S}(0) = \hat{S}_3 = 0\hat{S}_1 + 0\hat{S}_2 + 1\hat{S}_3. \quad (9.21)$$

Because rotations preserve the norm of vectors, as the direction of the magnetic field is changed, the spin operator will undergo rotations: however, the norm

$$|\hat{S}(t)|^2 = (s_1)^2 + (s_2)^2 + (s_3)^2 = 1 \quad (9.22)$$

will be preserved (see Fig. 9.1). The vector representing the spin thus moves on the surface of a sphere: the Bloch sphere [124]. So by applying some abstract group theory and Lie algebra results, we have obtained something very familiar to atomic physicists! However, as I have pointed out before, this effort will not be for naught: the language described above will enable us to form a very clear correspondence between the Bloch sphere and the geometric phase. Furthermore, the above language is generalizable, and will enable us to construct “pictures” similar to the Bloch sphere picture for more general groups of unitary transformations. These “pictures” will be useful for the same reason that the Bloch sphere is useful: they enable us to develop an intuitive understanding of complicated system dynamics.

Now, the system Hamiltonian for our spin-1/2 particle is proportional to  $\hat{S}_3$  and the initial state is an eigenstate of this operator. For this reason, the initial Hamiltonian does not cause any movement of the vector on the Bloch sphere but, rather, causes a trivial rotation about the axis of the vector itself. Of course, we can’t see the effect of this rotation on the vector. For this reason, it is useful to construct an orthonormal frame on the surface of the Bloch sphere, with the 3-axis normal to the surface, and (for example) the other two axes initially parallel to the 1- and 2-axes ( $x$ - and  $y$ -axes). The effect of the initial Hamiltonian ( $\propto \hat{S}_3$ ) is then to rotate this coordinate frame about its 3-axis.

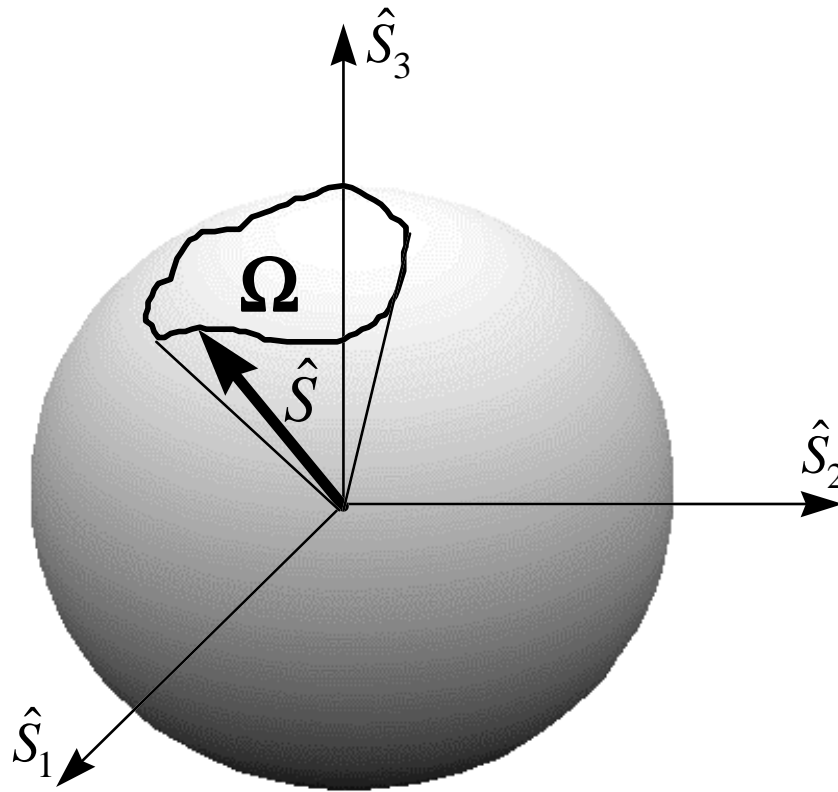


Figure 9.1: Rotations of a spin-1/2 particle in a magnetic field. The group of rotations moves  $\hat{S}_3$  on the surface of a sphere: it preserves the “length” of the vector in the three-dimensional vector space spanned by  $\hat{S}_1$ ,  $\hat{S}_2$ , and  $\hat{S}_3$ . The sphere is just the Bloch sphere.

By looking at the rotation of the coordinate axes tangent to the sphere’s surface (the 1- and 2-axes), we can keep track of the phases: for example, the “dynamical” phase due to  $\hat{U}(t) = e^{-i\hat{H}t/\hbar}$ . More generally, we shall allow the vector representing the state to move about the Bloch sphere, by changing the direction of the magnetic field. At each instant, the magnetic field will cause a rotation about its direction. However, this rotation of the state is, in some sense, trivial: it does not actually move the vector on the sphere. In general, we shall identify as a “dynamical” phase any contribution due to

an explicit rotation about the normal axis to the sphere: i.e. due to any transformation generated by an operator proportional to the vector which is representing the state. The interesting, “geometrical” phase is caused by the inherent curvature of the Bloch sphere. As in the classical, physical example of Sec. 9.1, even if we move the state-representing vector so as to eliminate any dynamical phase contribution (i.e. parallel transport it on the surface of the sphere), there will still be a net rotation of the coordinate frame, and hence a phase, due to this inherent curvature.

Thus, the distinction between dynamical and geometric phases is that the dynamical phase causes a rotation about the instantaneous direction of the vector representing the state (i.e. it is due to the instantaneous Hamiltonian). The geometric phase is the additional phase due to the rotation of coordinate frames as they are parallel-transported around the sphere, caused by the underlying geometry of the group producing the dynamics. This distinction is pointed out, in group theoretical notation and without the “picture” derived above, by Jordan [213]. So, even if the unitary rotations induce purely parallel transport of the vector around the sphere and back to the 3-axis, there can still be a net, geometrical phase, due to the inherent curvature: that is, the “anholonomy.”

To highlight the effects of the geometric phase in the system’s evolution, let us consider the case where the dynamical phase is zero: that is, in the geometric picture, we demand that

$$\hat{G}(t) \cdot \hat{S}(t) = 0. \quad (9.23)$$

From Eqs. (9.11) and (9.12), we have that

$$i \frac{d}{dt} \hat{S}(t) = [\hat{G}(t), \hat{S}(t)] \quad (9.24)$$

which, in the vector picture, can be expressed as:

$$\frac{d}{dt} \hat{S}(t) = \hat{G}(t) \times \hat{S}(t). \quad (9.25)$$

This is just the Bloch equation. In order to calculate the geometrical phase, we need to calculate the net phase in transporting the vector in a closed loop from the north

pole of the sphere back to the north pole. The way to do this is to consider a frame of coordinate axes on the surface of the sphere which moves with the state-representing vector, and to measure how much the  $x$ - and  $y$ -axes rotate in moving this frame around the closed loop. This angle will be the geometric phase.

Calculation of the rotation angle (the anholonomy) is a problem in differential geometry, but the calculation is relatively straightforward. A point on the unit sphere may be described by the triad  $(\sin \theta \cos \phi, \sin \theta \sin \phi, \cos \theta)$ , and we may prescribe a path on the sphere by appropriately specifying the parameters  $\theta$  and  $\phi$ . We may construct a coordinate frame at each point on the sphere by differentiating the  $x$ - and  $y$ -coordinates to obtain two vectors in the tangent plane, then taking the cross product of these two vectors to obtain a normal. Performing this procedure, we obtain:

$$\begin{aligned} \mathbf{f}_1 &= (\sin \theta \cos \phi, \sin \theta \sin \phi, \cos \theta) && \text{(normal vector)} \\ \mathbf{f}_2 &= (\cos \theta \cos \phi, \cos \theta \sin \phi, -\sin \theta) && \text{(direction of increasing } \theta) \\ \mathbf{f}_3 &= (-\sin \phi, \cos \phi, 0) && \text{(direction of increasing } \phi). \end{aligned} \tag{9.26}$$

So the quantity which we wish to measure is the angle  $\omega_{3,2}$  which, for example,  $\mathbf{f}_3$  moves towards  $\mathbf{f}_2$  as we go around the closed loop. From Eqs. (9.26), we have:

$$d\mathbf{f}_3 = (-\cos \phi d\phi, -\sin \phi d\phi, 0) \tag{9.27}$$

so that the desired change is

$$\omega_{3,2} = d\mathbf{f}_3 \cdot \mathbf{f}_2 = -\cos \theta d\phi. \tag{9.28}$$

The total rotation of the coordinate system is then given by the integral of  $\omega_{3,2}$  around the curve, or:

$$\gamma = \int_{\alpha} \omega_{3,2}, \tag{9.29}$$

where  $\alpha$  is a parametrization of the closed curve. (Note that  $\omega_{3,2}$  already contains a differential.) In the language of modern differential geometry  $\omega_{3,2}$  is a so-called “connection one-form” [218], and it is a general result of differential geometry that, if  $\Theta$  is

a one-form, then

$$\oint_{\alpha} \Theta = \iint_{\mathcal{S}} d\Theta \quad (9.30)$$

where  $\mathcal{S}$  is the area on the surface enclosed by the closed path  $\alpha$  and  $d\Theta$  is the differential of the one-form  $\Theta$ . This is just the generalization of Stokes' theorem. Another result from differential geometry is that  $d\omega_{3,2} = K \Theta_3 \wedge \Theta_2$  where  $K$  is the Gaussian curvature and  $\Theta_i$  are the unit one-forms (unit differentials) in the  $i^{\text{th}}$  frame direction<sup>5</sup>. For a sphere,  $K$  is equal to the curvature  $1/r^2$  of the sphere. In our case, since we are dealing with the unit sphere,  $K = 1$ . Finally, we can put all this together to obtain:

$$\gamma = \iint_{\mathcal{S}} \sin \theta \, d\theta d\phi, \quad (9.31)$$

which is just the solid angle subtended by the circuit, as seen from the sphere's origin.

In summary, then, the Berry's phase or geometric phase due to circumscribing some path on the sphere which begins and ends on the 3-axis (north pole) of the sphere is just equal to the area on the surface of the sphere. That is, the geometric angle is equal to the solid angle subtended by the path as seen from the origin.

If, as will generally be the case, Eq. (9.23) does *not* hold — that is,  $\hat{G}(t) \cdot \hat{S}(t) \neq 0$  — then the state will also pick up a dynamical phase. This phase is just given by the integral of the component of the generator at each point along the path which is parallel to the state-representing vector at that point. That is, it is given by the integral:

$$\xi = \oint_{\alpha} \hat{G} \cdot \hat{S}. \quad (9.32)$$

### 9.3 SU(1,1) Berry's Phase with Squeeze Operators

Recall from Sec. 6.1.4 that the squeeze operator  $\hat{S}(\epsilon) = \exp[\frac{1}{2}(\epsilon^* \hat{a}^2 - \epsilon (\hat{a}^\dagger)^2)]$  (where  $\epsilon = Re^{2i\phi}$ ) squeezes the uncertainty in one rotated quadrature of the ion's motion and amplifies the uncertainty in the other. A sequence of squeezes can produce an observable geometric phase in a trapped ion's motional state, which I will now

<sup>5</sup>  $\wedge$  is the exterior product (generalized cross product)

discuss. This geometric phase arising from squeezings was first discussed by Chiao and Jordan [206]. However, in order to discuss the geometric phase, it is more convenient to express the squeeze operator using a slightly different notation. Thus, we write:

$$\hat{\mathcal{S}}(r, \theta) = e^{ir(\hat{K}_1 \cos \theta + \hat{K}_2 \sin \theta)}, \quad (9.33)$$

where

$$\hat{K}_1 = -\frac{i}{4}(\hat{a}\hat{a} - \hat{a}^\dagger\hat{a}^\dagger) \quad (9.34)$$

$$\hat{K}_2 = \frac{1}{4}(\hat{a}\hat{a} + \hat{a}^\dagger\hat{a}^\dagger). \quad (9.35)$$

Some algebra allows us to make the connection with the previous notation:

$$r = 2R \quad (9.36)$$

$$\theta = -2\phi. \quad (9.37)$$

Thus, we can see that  $\hat{K}_1$  generates squeezes along the  $z$ -axis of the  $z$ - $p$  plane, and  $\hat{K}_2$  generates squeezes at  $45^\circ$  to the  $z$  and  $p$  axes.  $\hat{K}_1$  and  $\hat{K}_2$  are, in fact, orthogonal to each other in their effect. (It is apparent that squeezes along  $z$  and  $p$  are not orthogonal to each other, since a squeeze along  $z$  is just an “anti-squeeze” along  $p$ .)

Along with

$$\hat{J}_3 = \frac{1}{4}(\hat{a}\hat{a}^\dagger + \hat{a}^\dagger\hat{a}) = \frac{1}{2}\left(\hat{n} + \frac{1}{2}\right), \quad (9.38)$$

$\hat{K}_1$  and  $\hat{K}_2$  form a Lie algebra, the algebra SU(1,1). The commutation relations which characterize this algebra are:

$$[\hat{K}_1, \hat{K}_2] = -i\hat{J}_3, \quad [\hat{K}_2, \hat{J}_3] = i\hat{K}_1, \quad [\hat{J}_3, \hat{K}_1] = i\hat{K}_2, \quad (9.39)$$

which may be written succinctly as

$$[\hat{K}_i, \hat{K}_j] = i\tilde{\varepsilon}_{ijk}\hat{K}_k \quad (9.40)$$

with

$$\tilde{\varepsilon} \doteq (-1)^{\delta_{k,3}}\varepsilon_{ijk}. \quad (9.41)$$

In this last equation, I have written  $\hat{K}_3 \equiv \hat{J}_3$ . This notation is somewhat ambiguous, but the use of  $\hat{J}_3$  is in keeping with the literature. These commutation relations are the same as for the generators of the Minkowski transformations in (2+1) dimensions (special relativity deals with Minkowski transformations in (3+1) dimensions). Thus, the group of transformations generated by these three operators, when acting on a vector  $\mathbf{v} = v_1\mathbf{e}_1 + v_2\mathbf{e}_2 + v_3\mathbf{e}_3$ , preserve the ‘‘Minkowski dot product:’’

$$-(v_1)^2 - (v_2)^2 + (v_3)^2 = \text{const.} \quad (9.42)$$

As with the SU(2) example in the last section, the group generated by the SU(1,1) operators induces a geometry on the Lie algebra, when this algebra is considered as a vector space. Again, the structure constants  $\tilde{\varepsilon}_{ijk}$  provide the means to discover this geometry. So, writing general members of the Lie algebra/vector space as

$$\begin{aligned} \hat{K}_a &= (k_a)_1\hat{K}_1 + (k_a)_2\hat{K}_2 + (k_a)_3\hat{K}_3 \\ \hat{K}_b &= (k_b)_1\hat{K}_1 + (k_b)_2\hat{K}_2 + (k_b)_3\hat{K}_3 \\ \text{etc.} \dots & \end{aligned} \quad (9.43)$$

we have:

$$\begin{aligned} \hat{K}_a \tilde{\times} \hat{K}_b &= \hat{K}_c, \\ (k_c)_m &= (k_a)_l (k_b)_l \tilde{\varepsilon}_{lmn}. \end{aligned} \quad (9.44)$$

and

$$\begin{aligned} \hat{K}_a \tilde{\times} \hat{K}_b &= (K_a)_l (K_b)_m \tilde{\delta}_{lm} \\ \tilde{\delta}_{lm} &= -\frac{1}{2} \tilde{\varepsilon}_{lst} \tilde{\varepsilon}_{mts} \\ &= -\delta_{l,m} (-1)^{\delta_{l,3}}. \end{aligned} \quad (9.45)$$

In this language, the unitary transformations generated by SU(1,1) preserve the norm  $\hat{K} \tilde{\times} \hat{K}$ . This is just another way of expressing Eq. (9.42).

Now consider that we have a harmonic oscillator, and we initially start out in an eigenstate  $|n\rangle$  of that harmonic oscillator. This is also an eigenstate of  $\hat{K}(0) = \hat{J}_3 = \frac{1}{2}\hat{H}$ . If we apply a sequence of unitary transformations generated by  $\hat{K}_1$ ,  $\hat{K}_2$ , and  $\hat{J}_3$ , then, starting with  $\hat{J}_3$ :

$$\hat{K}(0) \longrightarrow \hat{K}(t) = k_1(t)\hat{K}_1 + k_2(t)\hat{K}_2 + k_3(t)\hat{J}_3. \quad (9.46)$$

That is, the unitary transformations take the vector  $\hat{J}_3$  into a linear combination of the basis vectors  $\hat{K}_1$ ,  $\hat{K}_2$ , and  $\hat{J}_3$  of the vector space. Since the unitary operators are generated by the SU(1,1) algebra, we have that, in the course of this evolution:

$$\hat{K}(t)\tilde{\hat{K}}(t) = -k_1(t)^2 - k_2(t)^2 + k_3(t)^2 = 1, \quad (9.47)$$

since we initially have  $-k_1(0)^2 - k_2(0)^2 + k_3(0)^2 = -0^2 - 0^2 + 1^2 = 1$ . So, in the course of the system's evolution, the vector which starts out as  $\hat{J}_3$  (i.e. along the  $k_3$  or  $\hat{J}_3$  axis) moves along the surface of the unit hyperboloid, as shown in Fig. 9.2.

As before, we may describe the time evolution of  $\hat{U}(t)$  and hence of  $\hat{K}(t)$ , given some sequence of generators  $\hat{G}(t) = g_1(t)\hat{K}_1 + g_2(t)\hat{K}_2 + g_3(t)\hat{J}_3$ . We have that

$$\hat{K}(t) = \hat{U}(t)\hat{K}(0)\hat{U}^\dagger(t) = \hat{U}(t)\hat{J}_3\hat{U}^\dagger(t), \quad (9.48)$$

$$i\frac{d}{dt}\hat{U}(t) = \hat{G}(t)\hat{U}(t), \quad (9.49)$$

and hence:

$$i\frac{d}{dt}\hat{K}(t) = [\hat{G}(t), \hat{K}(t)]. \quad (9.50)$$

In the vectorial picture, Eq. (9.50) becomes

$$\frac{d}{dt}\hat{K}(t) = \hat{G}(t)\tilde{\times}\hat{K}(t), \quad (9.51)$$

which is the equivalent of the Bloch equation.

If we apply a sequence of such transformations such that, at time  $t = \tau$ , we end up with  $\hat{K}(\tau)$  again along the positive  $\hat{J}_3$  axis (at the nadir of the hyperboloid), then,

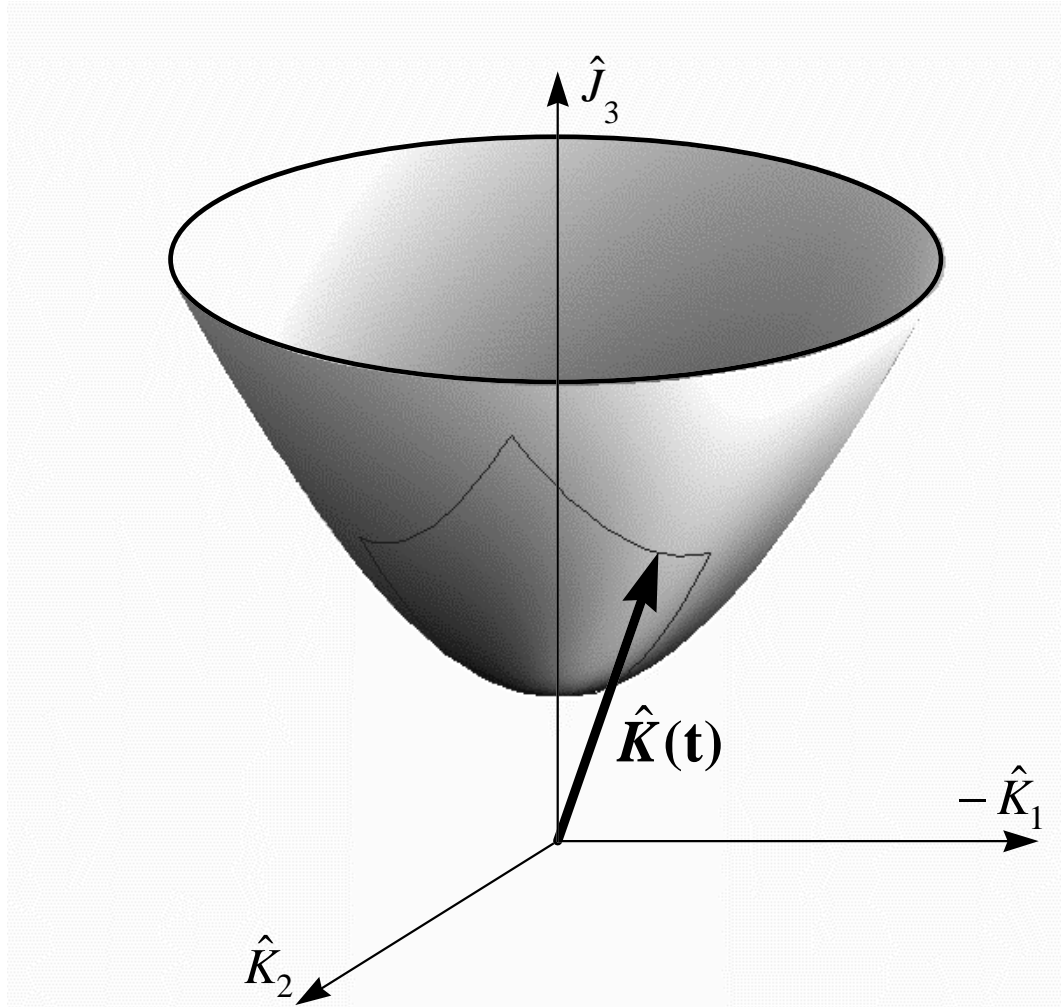


Figure 9.2: Unit hyperboloid in the vector space spanned by  $\hat{J}_3 = \frac{1}{4}(\hat{a}\hat{a}^\dagger + \hat{a}^\dagger\hat{a})$ ,  $\hat{K}_1 = -\frac{i}{4}(\hat{a}\hat{a} - \hat{a}^\dagger\hat{a}^\dagger)$ , and  $\hat{K}_2 = \frac{1}{4}(\hat{a}\hat{a} + \hat{a}^\dagger\hat{a}^\dagger)$ . An initial state  $\hat{J}_3$  moves on the surface of this hyperboloid under the (squeezing and rotation) operations generated by these three operators. This hyperboloid is a useful tool for visualizing the effects of these transformations upon an eigenstate of  $\hat{J}_3$  (i.e. of  $\hat{n}$ ), just as the Bloch sphere is useful in visualizing spin rotations. The path indicated on the surface of the hyperboloid is that traced out in the experiment discussed in the text.

in the course of that evolution,

$$\hat{J}_3 \longrightarrow e^{i\phi\hat{J}_3} \hat{J}_3 \quad (9.52)$$

and, just as in the spin/magnetic field case, we pick up a phase factor:

$$|\psi\rangle_0 = |n\rangle \longrightarrow |\psi\rangle_\tau = e^{i\phi\hat{J}_3} |n\rangle = e^{i(n+\frac{1}{2})\phi/2} |n\rangle. \quad (9.53)$$

We may calculate the dynamical and geometric contributions to the phase  $\phi = \xi + \gamma$  as in the last section, if we merely replace the dot and cross products there by their Minkowski space equivalents. Thus,

$$\xi = \int_0^\tau \hat{G}(t') \cdot \hat{K}(t') dt' . \quad (9.54)$$

In order to calculate the geometric phase, we need to calculate the surface area on the hyperboloid enclosed by the path traced out by  $\hat{K}(t)$ , in the Minkowski metric. Using  $k_1$ ,  $k_2$ , and  $k_3$  as our coordinates, and applying the constraint that  $-(k_1)^2 - (k_2)^2 + (k_3)^2 = 1$ , we have that the element of surface area on the unit hyperboloid is given by

$$d\mathcal{S} = \frac{dk_1 dk_2}{k_3} = \frac{dk_1 dk_2}{\sqrt{1 + k_1^2 + k_2^2}} \quad (9.55)$$

and so

$$\gamma = \oint_{\mathcal{S}} \frac{dk_1 dk_2}{\sqrt{1 + k_1^2 + k_2^2}}, \quad (9.56)$$

where  $\mathcal{S}$  is the surface enclosed by the path traced out by  $\hat{K}(t)$ .

The geometric phase induced by  $SU(1,1)$  dynamics has been measured before. Kitano and Yabuzaki [223] measured the net rotation in the polarization of light passed through a network of linear polarizers. This net rotation can be expressed in terms of the geometric phase<sup>6</sup>. Svensmark and Dimon [224] measured a phase shift in a series of connected, nonlinear oscillators. However, in both these cases, the measurements were performed on *classical* electric fields. It is, therefore, of some interest to measure

---

<sup>6</sup> if one ignores the losses in the polarizers, which induce non-unitary, rather than unitary, evolution.

the geometric phase in the *wave function* of a material oscillator. Furthermore, in our system, we have the unique ability to prepare Fock states and thus to measure the  $(n + \frac{1}{2})/2$  Fock state dependence of the geometry phase.<sup>7</sup>

The basic idea for measuring the geometric phase in our system is to perform a Ramsey experiment on the spin, and perform a sequence of squeeze operations in between the Ramsey zones. The Ramsey experiment maps any relative motional phase between  $|\uparrow\rangle$  and  $|\downarrow\rangle$  onto the spin phase, which manifests itself as a shift in the Ramsey fringes. So, for example, if we do not squeeze or otherwise affect  $|\downarrow\rangle$ , but apply a sequence of operations on the motional state in  $|\uparrow\rangle$  corresponding to a closed path on the unit hyperboloid, we could measure Berry's phase as the phase shift between  $|\uparrow\rangle$  and  $|\downarrow\rangle$ . In the rotating frame, any contribution to the phase shift from the “natural” motional time evolution drops out, and the only contribution comes from the effects of the operators applied between the Ramsey zones.

There are, of course, many possible closed paths on the unit hyperboloid. For instance, we might imagine applying a squeeze generated by  $\hat{K}_1$ , rotating the vector by  $\pi/2$  radians by applying  $e^{i\pi\hat{J}_3/2}$ , then undoing the squeeze by applying a squeeze generated by  $\hat{K}_2$  [225]. However, we do not (in the rotating frame) have an experimental implementation of a pure “phase space rotation” ( $\hat{J}_3$ ) operator. The most straightforward procedure<sup>8</sup> is to apply a sequence of four squeezes [206]:

$$e^{ir\hat{K}_2}e^{is\hat{K}_1}e^{-is\hat{K}_2}e^{-ir\hat{K}_1}. \quad (9.57)$$

Of course, in order to circumscribe a closed area on the unit hyperboloid,  $r$  and  $s$  must satisfy some relationship between each other. One might expect that we require  $r = s$ , but this is not the case. The reason for this is that the effects of a squeeze operator

<sup>7</sup> Since  $\exp(-i\gamma\hat{J}_3)\hat{a}\exp(i\gamma\hat{J}_3) = \exp(i\gamma/2)\hat{a}$ , all coherent states pick up the same phase  $\exp(i\gamma/2)$ .

<sup>8</sup> Actually, one may trace out a closed path on the unit hyperboloid with a sequence of *three* pure squeezes: for example  $\exp(ir\hat{K}_1)\exp[i(a\hat{K}_1 + b\hat{K}_2)]\exp(-is\hat{K}_2)$ . However, the algebraic relations between  $r$ ,  $s$ ,  $a$ , and  $b$  are somewhat complex (though numerically soluble). In fact, as we shall see, there are reasons for performing a sequence of *four* squeezes: simplicity and the ability to “split the job up” between  $|\uparrow\rangle$  and  $|\downarrow\rangle$ .

depend on where on the hyperboloid it is applied. An analogous effect happens with a vector whose tip is constrained to move on the surface of a sphere: near the north pole, a rotation of  $\pi/2$  radians about the 3-axis moves the vector's tip only a small arc length. Further from the north pole, however, a rotation by the same angle moves the tip of the vector by a much greater arc length. In our case, on the unit hyperboloid, the condition for the four squeezes listed above to move the vector in a closed path is that [206]

$$\sinh s = \tanh r. \quad (9.58)$$

Under the above evolution, the dynamical phase is given by:

$$\xi = \int_0^\tau \hat{K}(t') \hat{G}(t') dt' = 2 \operatorname{arcsinh}[\tanh r] \sinh r. \quad (9.59)$$

The geometric phase is given by:

$$\gamma = - \int_{k_1=0}^{\sinh r} \int_{k_2=0}^{\sinh r} \frac{dk_1 dk_2}{k_3} = -2 \operatorname{arcsinh}[\tanh r] \sinh r + \arcsin[\tanh^2 r] \quad (9.60)$$

(some details of the integration, which involves some obscure integrals, are given in Appendix C). The dynamical phase cancels out some of the geometric phase, and the net phase shift induced by the sequence of four squeezes is:

$$\phi = 2 \arcsin[\tanh^2 r]. \quad (9.61)$$

The dynamic, geometric, and net phase shift are shown in Fig. 9.3. Note that the net phase shift reaches its maximum value for  $r \approx 3$ , corresponding to  $R \approx 1.5$ .

## 9.4 Experimental Issues

Ideally, then, we would perform an experiment in which we prepared an equal superposition of  $|\uparrow\rangle$  and  $|\downarrow\rangle$ , performed the sequence (9.57) of four squeezings on the  $|\uparrow\rangle$  part of the motional state only, and then compare the phase of the  $|n=0\rangle$  state in  $|\downarrow\rangle$  with the  $|n=0\rangle$  result of squeezing  $|\uparrow\rangle$ , by recombining the  $|\uparrow\rangle$  and  $|\downarrow\rangle$  wave

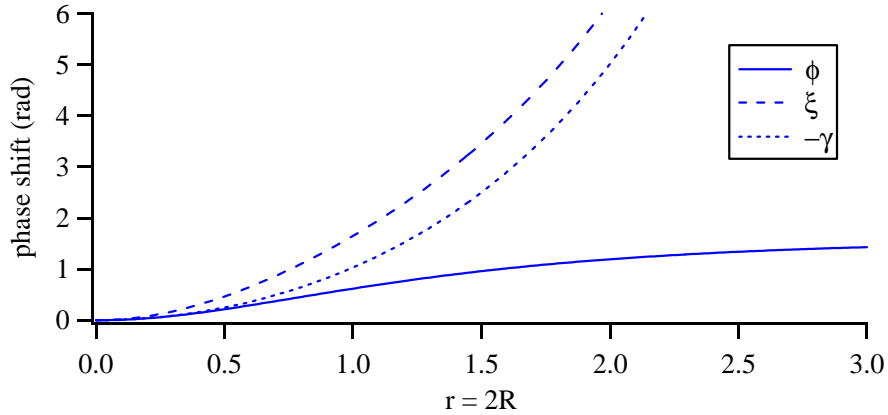


Figure 9.3: (a) Predicted phase shift for an initial  $|n = 0\rangle$  state subject to a sequence of four squeezings constituting a closed path on the unit hyperboloid.  $\gamma$  is the geometric contribution to the phase, due to the inherent curvature of the hyperboloid upon which moves the vector which represents the state.  $\xi$  is the dynamical phase. The net phase is  $\phi$ .

packets. The net phase shift  $\phi$  resulting from the residual geometric phase (Eq. (9.61)) would then result in a net phase shift of the Ramsey fringes with respect to the usual Ramsey experiment in which the four squeeze pulses were absent. This experiment is attractive, since we may “peak up” the four squeeze operators by applying them to the state  $|\uparrow\rangle$  and confirming that we return to the motional state  $|n = 0\rangle$ .

However, the squeeze operators which are produced by the “walking standing wave” interaction with the laser beams (Sec. 6.1.4) are of second order in the Lamb-Dicke parameter  $\eta$  and so, the squeezing operations are relatively slow. We attempted to measure the SU(1,1) Berry’s phase in the micromachined linear ion trap. Unfortunately, the background heating rate precluded performing four sequential squeeze operations: the decoherence washed out any signal. This did not present an insurmountable barrier, however. As pointed out by Chiao and Jordan [206] in a different context, it suffices to perform two squeezes on one part of the spin wave packet and the other two on the other part. Thus, an equivalent experiment consists of a  $\pi/2$  carrier pulse, simultaneously

performing the operations:

$$|\downarrow, 0\rangle \longrightarrow e^{-is\hat{K}_2} e^{-ir\hat{K}_1} |\downarrow, 0\rangle \quad (9.62)$$

$$|\uparrow, 0\rangle \longrightarrow e^{-is\hat{K}_1} e^{-ir\hat{K}_2} |\uparrow, 0\rangle. \quad (9.63)$$

Then the Ramsey experiment measures the overlap

$$\langle 0 | e^{ir\hat{K}_2} e^{is\hat{K}_1} e^{-is\hat{K}_2} e^{-ir\hat{K}_1} | 0 \rangle, \quad (9.64)$$

just as in the original experiment. The trick, however, is to arrange that a squeeze  $e^{ir\hat{K}_1}$  on  $|\downarrow\rangle$  should be a squeeze  $e^{ir\hat{K}_2}$  on  $|\uparrow\rangle$ . It is possible to do this, by appropriately setting the polarization of the Raman beams, as described below.

#### 9.4.1 Differential Squeezing Using Polarization

Recall from Sec. 6.1.4 that the squeeze parameter for “walking standing wave” production of squeezed states is given by  $\epsilon = R e^{2i\phi} = \frac{r}{2} e^{i\theta} = i\eta^2 \Omega t e^{i\phi_L}$  (where I have now explicitly written the laser phase). But, as discussed in Sec. 6.2.1, the effective Rabi frequencies for  $|\uparrow\rangle$  and  $|\downarrow\rangle$  for the “walking standing wave” interaction depend on the polarizations of the two Raman beams creating the interaction. As discussed there,  $R_{co}$  must have the polarization  $\frac{1}{\sqrt{2}}(\sigma^+ + \sigma^-)$ , but we may alter the polarization of the  $RR_{\perp}$  beam. Recall Eqs. (6.19) and (6.20):

$$\begin{aligned} \Omega_{\downarrow} &= \frac{g^2}{\Delta_R + \omega_0} \frac{2\Upsilon}{3} + \frac{g^2}{\Delta_R + \delta_{FS} + \omega_0} \left( \Lambda + \frac{\Upsilon}{3} \right) \\ \Omega_{\uparrow} &= \frac{g^2}{\Delta_R} \left( \frac{\Lambda}{2} + \frac{\Upsilon}{6} \right) + \frac{g^2}{\Delta_R + \delta_{FS}} \left( \frac{\Lambda}{2} + \frac{5\Upsilon}{6} \right), \end{aligned}$$

where the  $RR_{\perp}$  beam has polarization  $\Lambda\sigma^- + \Upsilon\sigma^+$ . In Sec. 6.2.1, we ignored the hyperfine splitting when deriving Eq. (6.21) for the ratio of  $\Omega_{\downarrow}$  to  $\Omega_{\uparrow}$ . Now, if we take this into account, we obtain:

$$\frac{\Omega_{\downarrow}}{\Omega_{\uparrow}} = \frac{\Delta_R (\delta_{FS} + \Delta_R) \left( \frac{4\Upsilon}{\omega_0 + \Delta_R} + \frac{2(3\Lambda + \Upsilon)}{\delta_{FS} + \omega_0 + \Delta_R} \right)}{3\Lambda + \delta_{FS}\Upsilon + 6(\Lambda + \Upsilon)\Delta_R}. \quad (9.65)$$

By placing a  $\frac{\lambda}{4}$  followed by a  $\frac{\lambda}{2}$  plate in the  $\overline{\text{RR}}_{\perp}$  beam line immediately before the input lens to the trap envelope, we can choose any value for  $\Lambda$  and  $\Upsilon$ . We want to realize the operator  $\hat{S}(r, \theta = 0) = e^{ir\hat{K}_1}$  in one spin state, and the operator  $\hat{S}(r, \theta = \pi/2) = e^{ir\hat{K}_2}$  in the other. It follows from Eq. (6.17), therefore, that we want to have

$$\frac{\Omega_{\downarrow}}{\Omega_{\uparrow}} = \pm i. \quad (9.66)$$

The values of  $\Lambda$  and  $\Upsilon$  are somewhat complicated functions of the angles of the  $\frac{\lambda}{4}$  and  $\frac{\lambda}{2}$  plate angles, and the dependence of the Rabi frequency ratio, through Eq. (9.65), even more complicated. Nonetheless, the resulting equation can be solved numerically (for a given Raman beam detuning  $\Delta_R$ ) to obtain the angles. For example, at a detuning of  $\Delta_R = 12.33$  GHz, the the slow axis of the quarter-wave plate should be at  $-6.1^\circ$  from the vertical and the slow axis of the half-wave plate at  $-31.9^\circ$  from the vertical (assuming a vertically polarized input beam).

Figure 9.4(a), (b), and (c) show the dependence of the absolute value and argument of the ratio  $\frac{\Omega_{\downarrow}}{\Omega_{\uparrow}}$  as a function of  $\Delta_R$ , the  $\frac{1}{4}$ -wave plate angle, and the  $\frac{1}{2}$ -wave plate angle, the other parameters being held fixed at their nominal values. These figures indicate that, although care must be taken in setting the wave plate angles, the requirements for appropriate squeezing of  $|\uparrow\rangle$  and  $|\downarrow\rangle$  are not impracticable.

Unfortunately, birefringence in the vacuum envelope windows added a random change in the polarization of the  $\overline{\text{RR}}_{\perp}$  beam after the polarization optics. This birefringence also varied from spot to spot on the windows. Since the “peaking up” procedure involved comparing squeezed state flopping curves for initial  $|\uparrow, n = 0\rangle$  and  $|\downarrow, n = 0\rangle$  curves,<sup>9</sup> a time-consuming procedure, it was not practical to perform the experiment, given the unknown birefringence of the windows. Unfortunately, since there was one window between the polarization optics and the ion, but two windows before the beam

---

<sup>9</sup> Other meters of the relative squeezing in  $|\uparrow\rangle$  and  $|\downarrow\rangle$  exist — for example, variants of the Ramsey experiment. Several such techniques were tried: however, the heating-induced decoherence made them essentially useless with the ion heating at the rate it did when the experiments were tried.

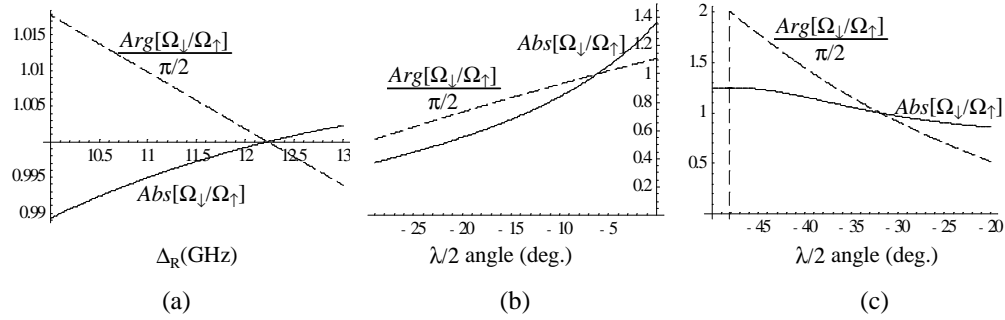


Figure 9.4: Sensitivity of  $\Omega_{\downarrow}/\Omega_{\uparrow}$  to errors in experimental parameters. Nominal values for  $\Omega_{\downarrow}/\Omega_{\uparrow} = i$  are  $\Delta_R = 12.333$  GHz,  $\frac{\lambda}{4}$  plate at  $-6.1^\circ$  from the vertical, and  $\frac{\lambda}{2}$  plate at  $-31.9^\circ$  from the vertical. (a) Dependence of  $\Omega_{\downarrow}/\Omega_{\uparrow}$  on the detuning  $\Delta_R$  of the Raman beams from the  $2p^2P_{1/2}$  virtual level, with the quarter- and half-wave plate angles held at their nominal values. The detuning affects the relative importance of transitions driven through the  $^2P_{1/2}$  and  $^2P_{3/2}$  (virtual) levels. (b) Dependence of  $\Omega_{\downarrow}/\Omega_{\uparrow}$  on the angle of the quarter-wave plate, with  $\Delta_R = 12.333$  GHz and the half-wave plate held at its nominal value. (c) Dependence of  $\Omega_{\downarrow}/\Omega_{\uparrow}$  on the angle of the half-wave plate, with  $\Delta_R = 12.333$  GHz and the quarter-wave plate held at its nominal value. In (a), (b), and (c), the dashed lines show the argument of the complex Rabi frequency ratio, while the solid lines show its magnitude.

passed out the other side of the vacuum envelope, it was not possible to determine the polarization state at the ion.

Were the heating rate lower, all four squeezes could be performed on only one of the spin states. In this case (neglecting the fine-structure contributions, which is a small perturbation for small  $\Delta_R$ ), as with the original Schrödinger cat experiment, pure  $\sigma^-$  light in the  $RR_{\perp}$  beam line would affect only  $|\downarrow\rangle$ . Despite the birefringence in the windows, there are rapid diagnostics which could allow us to determine when the light at the ion is pure  $\sigma^-$ : for example, the cycling transition (see Appendix A). Thus, if the heating rate were low enough to allow four sequential squeeze operations, the experiment would be possible.

### 9.4.2 The Effect of Small Errors on Berry's Phase

It is worthwhile to examine the effects of small errors in the squeeze operations on the measured residual geometric phases. For example, the magnitude of the Rabi frequencies in  $|\uparrow\rangle$  and  $|\downarrow\rangle$  might not be equal, or the argument between the two might not be exactly  $\pi/2$  radians. Alternatively, in a four-squeeze implementation, there might be slight errors in the magnitudes of the squeezes. In general, since the geometry of the unit hyperboloid (see above) is smooth, we would not expect a small imperfection in the path of the vector representing the state to translate into very large changes in the observed phase. Of course, if the path on the hyperboloid is not closed, it is not possible to talk of the solid angle enclosed by that path. However, different approaches to the issue are possible.

One approach which facilitates the determination of the effects of small errors uses yet another description of the phase shifts which occur in applying sequential squeezings. This approach arises from considering the action of two sequential squeezing operations, as was considered in Refs. [226, 227]. Before writing down the result, it is worthwhile to reiterate the effects of the group elements generated by the  $SU(1,1)$  algebra. The operator

$$\hat{R}(\zeta) = e^{i\zeta\hat{J}_3} = e^{i\zeta(\hat{a}\hat{a}^\dagger + \hat{a}^\dagger\hat{a})/4} \quad (9.67)$$

produces “rotations” in phase space. (In our case, since there is only one “dimension” in which rotations may occur, rotation operators commute.) The operator

$$\hat{S}(r, \vartheta) = e^{ir(\hat{K}_1 \cos \vartheta + \hat{K}_2 \sin \vartheta)} \quad (9.68)$$

generates a squeeze along the direction  $\vartheta/2$ . In general, we may re-express Eq. (9.68) as:

$$\hat{S}(r, \vartheta) = \hat{R}^\dagger(\vartheta)\hat{S}(r, 0)\hat{R}(\vartheta). \quad (9.69)$$

The result of two squeezes is then a squeeze plus a rotation. Specifically [226, 227],

$$\hat{\mathcal{S}}(p, \zeta)\hat{\mathcal{S}}(q, 0) = \hat{R}(\Phi)\hat{\mathcal{S}}(r, \vartheta'), \quad (9.70)$$

where

$$r = \operatorname{arccosh} [\cosh p \cosh q + \cos \zeta \sinh p \sinh q], \quad (9.71)$$

$$\vartheta' = \arctan \left\{ \frac{\sin \zeta \sinh p}{\sinh q \cosh p + \cos \zeta \sinh p \cosh q} \right\}, \quad (9.72)$$

$$\Phi = 2 \arctan \left\{ \frac{-\sin \zeta \sinh(p/2) \sinh(q/2)}{\cosh(p/2) \cosh(q/2) + \cos \zeta \sinh(p/2) \sinh(q/2)} \right\}. \quad (9.73)$$

Note that this result also holds true when considering the special relativity (in 2+1 dimensions) interpretation of the transformations generated by SU(1,1). In this language, rotations are rotations, squeezes are boosts, and the product of two boosts is a net boost *plus* a rotation. This is the origin of the Thomas precession (see Ref. [89]§11.8).

Recall from Eq. (9.57) that the experiment consists of the four operations

$$e^{ir\hat{K}_2} e^{is\hat{K}_1} e^{-is\hat{K}_2} e^{-ir\hat{K}_1} \equiv \hat{\mathcal{S}}(r, \frac{\pi}{2})\hat{\mathcal{S}}(s, 0)\hat{\mathcal{S}}(s, \frac{3\pi}{2})\hat{\mathcal{S}}(r, \pi). \quad (9.74)$$

Using Eq. (9.70) to combine the left two and right two squeeze operators, we may re-express this as:

$$\hat{\mathcal{S}}(r, \frac{\pi}{2})\hat{\mathcal{S}}(s, 0)\hat{\mathcal{S}}(s, \frac{3\pi}{2})\hat{\mathcal{S}}(r, \pi) = \hat{R}(\Phi_1)\hat{\mathcal{S}}(R_1, \vartheta_1)\hat{R}(\Phi_2)\hat{\mathcal{S}}(R_2, \vartheta_2), \quad (9.75)$$

where  $R_1$ ,  $R_2$ ,  $\vartheta_1$ ,  $\vartheta_2$ ,  $\phi_1$ , and  $\phi_2$  are obtained from Eq. (9.73). In fact, it is straightforward to show that  $R_1 = R_2 \doteq R$  and  $\Phi_1 = \Phi_2 \doteq \Phi$  for the prescribed sequence of squeezes, although  $\vartheta_1 \neq \vartheta_2$ . Thus,

$$\begin{aligned} \hat{\mathcal{S}}(r, \frac{\pi}{2})\hat{\mathcal{S}}(s, 0)\hat{\mathcal{S}}(s, \frac{3\pi}{2})\hat{\mathcal{S}}(r, \pi) &= \hat{R}(\Phi)\hat{\mathcal{S}}(R, \vartheta_1)\hat{R}(\Phi)\hat{\mathcal{S}}(R, \vartheta_2) \\ &= \hat{R}(\Phi)\hat{\mathcal{S}}(R, \vartheta_1)\hat{R}(\Phi - \vartheta_2)\hat{\mathcal{S}}(R, 0)\hat{R}(\vartheta_2) \\ &= \hat{R}(2\Phi - \vartheta_2)\hat{\mathcal{S}}(R, \vartheta_1 + \Phi - \vartheta_2)\hat{\mathcal{S}}(R, 0)\hat{R}(\vartheta_2). \end{aligned} \quad (9.76)$$

Now, if  $\vartheta_1 - \vartheta_2 + \Phi = \pi$ , the two squeezes on the last line cancel, and the net effect is a rotation operator

$$\hat{R}(2\Phi - \vartheta_2)\hat{R}(\vartheta_2) = \hat{R}(2\Phi). \quad (9.77)$$

This occurs if  $\tanh r = \sinh s$ , which is the same as Condition (9.58).<sup>10</sup> So another way of looking at the experiment is that, if we choose the squeeze parameters correctly, the resultant squeeze of the first two squeeze operators cancels with that of the second two, and we are left only with the net rotation (the equivalent of the Thomas precession). Of course, with this approach, we cannot distinguish between dynamical and geometric contributions to the resultant phase, which is the advantage of the approach taken in Sec. 9.3.

If we now assume that there are small errors in the experimental pulses, then the two squeeze operators will not exactly cancel. For example, suppose that the angles  $(0, \pi/2, \pi, \text{ and } 3\pi/2)$  of the various operations are correct, but that there are errors in the magnitude of the various squeezes. This is a reasonable model of the errors, since the phase between the squeezes will either be set by an rf phase or a polarizer setting — either of which may be well controlled. The squeeze amplitudes, however, may be harder to calibrate and keep constant. We may model this situation by assuming  $s$ , and letting  $r \rightarrow r + \varepsilon$  (where still  $\tanh r = \sinh s$ ). In this case, Eq. (9.76) becomes

$$\hat{S}(r + \varepsilon, \frac{\pi}{2})\hat{S}(s, 0)\hat{S}(s, \frac{3\pi}{2})\hat{S}(r + \varepsilon, \pi) = \hat{R}(2\Phi' - \vartheta'_2)\hat{S}(R', \vartheta'_1 + \Phi' - \vartheta'_2)\hat{S}(R', 0)\hat{R}(\vartheta'_2). \quad (9.78)$$

Note that combining the leftmost and rightmost pairs of squeeze operators still results in the same squeeze amplitude and rotation angle, as was the case before. Explicitly:

$$R' = \operatorname{arccosh} [\cosh(r + \varepsilon) \cosh s] \doteq R + \alpha \quad (9.79)$$

$$\Phi' = -2\arctan \{ \tanh[(r + \varepsilon)/2] \tanh[s/2] \} \doteq \Phi + \beta. \quad (9.80)$$

---

<sup>10</sup> It is extremely challenging to prove this algebraically. On the other hand, we can plug the result from Eq. (9.58) into the combined expressions for  $\vartheta_1 - \vartheta_2 + \Phi$  from Eq. (9.73) and verify the truth of the statement.

$\vartheta'_1$  and  $\vartheta'_2$  also differ from their values above. Explicitly:

$$\vartheta'_1 = \arctan \left[ \frac{\tanh(r + \varepsilon)}{\sinh s} \right] \doteq \vartheta_1 + \delta \quad (9.81)$$

$$\vartheta'_2 = \arctan \left[ \frac{\tanh s}{\sinh(r + \varepsilon)} \right] \doteq \vartheta_2 + \kappa. \quad (9.82)$$

One result is that  $\vartheta'_1 - \vartheta'_2 + \Phi' \neq \pi$ . Thus, the two squeeze operators resulting from the combination of the left pair and right pairs of squeezes no longer cancel. The result, according to Eq. (9.70), is an additional squeeze and an additional rotation over the ideal case. The phase shift which we measure then differs from the theoretical prediction, Eq. (9.61), for two reasons. First, the arguments of the outermost rotation operators in Eq. (9.78) no longer have the correct values. Second, the fact the the two squeeze operators in the middle of Eq. (9.78) no longer cancel introduces an *additional* rotation operator and, hence, an additional phase shift error. As well, the squeeze operator causes a reduction in the Ramsey fringe contrast.

The experiment measures, for example,  $\langle 0 | \hat{U} | 0 \rangle$  which, in the presence of the error is given by:

$$\begin{aligned} \langle 0 | \hat{R}(2\Phi' - \vartheta'_2) \hat{S}(R', \vartheta'_1 + \Phi' - \vartheta'_2) \hat{S}(R', 0) \hat{R}'(\vartheta'_2) | 0 \rangle \\ = e^{i\Phi'/2} \langle 0 | \hat{R}(\Lambda) \hat{S}(v, \nu) | 0 \rangle \\ = e^{i\Phi'/2} e^{i\Lambda/4} \frac{1}{\sqrt{\cosh v}} \\ = e^{i\Phi'/2} e^{i(\Lambda+\alpha)/4} \frac{1}{\sqrt{\cosh v}}. \end{aligned} \quad (9.83)$$

Here,  $v$  and  $\nu$  (which doesn't enter into the final result) are the parameters of the squeeze resulting from  $\hat{S}(R', \vartheta'_1 + \Phi' - \vartheta'_2) \hat{S}(R', 0)$  and  $\Lambda$  is the rotation angle.

Now, in the ideal case, we have  $\Phi + \vartheta_1 - \vartheta_2 = \pi$ . Thus, from Eqs. (9.80), (9.81), and (9.82), we have

$$\Phi' + \vartheta'_1 - \vartheta'_2 = \pi + \alpha + \delta - \kappa \quad (9.84)$$

so that

$$\sin(\Phi' + \vartheta'_1 - \vartheta'_2) = -\sin(\beta + \delta - \kappa)$$

$$\cos(\Phi' + \vartheta'_1 - \vartheta'_2) = -\cos(\beta + \delta - \kappa). \quad (9.85)$$

Using the above information in Eq. (9.70), we obtain:

$$\begin{aligned} v &= \operatorname{arccosh} \left[ \cosh^2(R + \alpha) - \cos(\beta + \delta - \kappa) \sinh^2(R + \alpha) \right] \\ \Lambda &= 2 \arctan \left\{ \frac{\sin(\beta + \delta - \kappa) \sinh^2[(R + \beta)/2]}{\cosh^2(R + \alpha)/2 - \cos(\beta + \delta - \kappa) \sinh^2[(R + \alpha)/2]} \right\} \end{aligned} \quad (9.86)$$

which we can plug back into Eq. (9.83) to determine the effect on the measured signals. Of course, if we do this, we only express the error in terms of  $\alpha$ ,  $\beta$ ,  $\delta$ , and  $\kappa$ : the errors in the parameters  $R$ ,  $\Phi$ ,  $\vartheta_1$ , and  $\vartheta_2$  of the combined squeezes. In order to express the error in terms of  $\varepsilon$  (the error in the squeeze parameter  $r$ ), we need to use the full expressions in Eqs. (9.80), (9.81), and (9.82). This is straightforward. However, the algebra is complicated enough that performing this final step adds little to the information content of this description. I shall, therefore, merely quote the result.

Figure 9.5 plots the net phase for the ideal Berry's phase experiment and with  $\varepsilon = 0.05r$  — that is to say,  $r \rightarrow 1.05 \operatorname{arctanh}[\sinh s]$ . For small squeeze parameters, small errors in the squeeze operations should result in small errors in the measured phase shift.

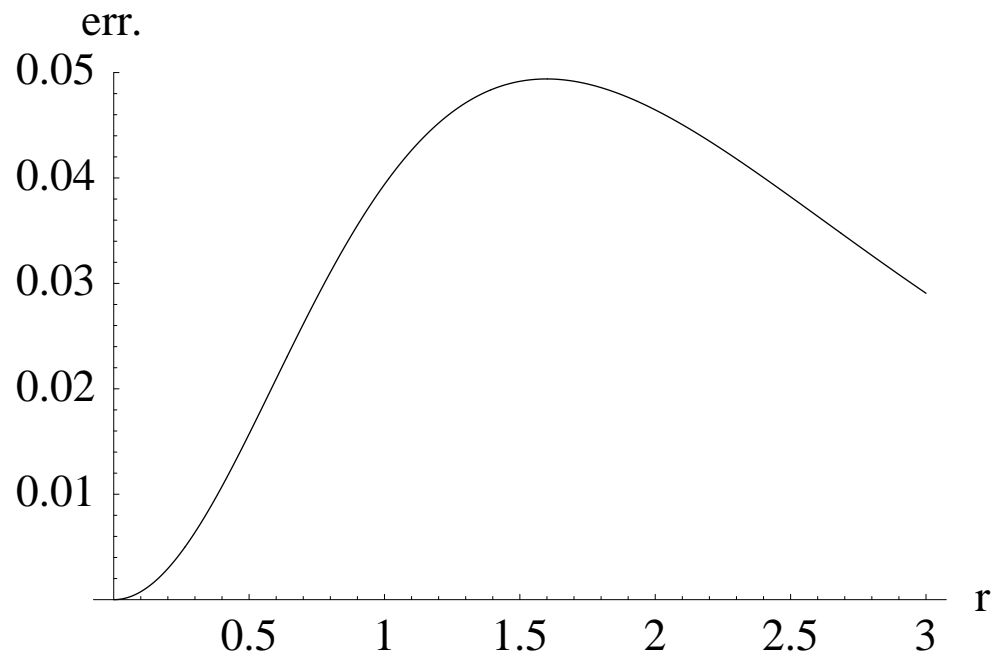


Figure 9.5: Effect of small imperfections of the squeezing pulses on the measured geometric phase shift. The curve shows the absolute error, assuming a five percent error in  $r$ , the amplitude of the first squeeze. The ordinate axis shows  $r$ , but in the various formulae for the phase shift,  $r \rightarrow 1.05 r$ . However, the amplitude  $s$  of the second squeeze satisfies  $\tanh r = \sinh s$ , where  $r$  is read off the ordinate axis of the graph.